

Investigation on the Tensile Strength and Microhardness of AA6061/TiC Composites by Stir Casting

J. Jebeen Moses¹ · S. Joseph Sekhar¹

Received: 4 November 2015 / Accepted: 29 April 2016 / Published online: 14 May 2016
© The Indian Institute of Metals - IIM 2016

Abstract AA6061 is widely used in aircraft, marine and automobile industries for its high strength to weight ratio, good ductility and corrosion resistance. The stir casting process parameters play a vital role in deciding the particle dispersion and the mechanical strength of the composites. In this paper, an attempt has been made to develop the empirical relationship to predict tensile strength and microhardness of the AA6061 reinforced with TiC by incorporating the process parameters such as stirrer blade angle (α), stirring speed (N) and stirring time (T) whose values were optimized. Three factors, five level central composite design has been used to minimize the number of experimental conditions. Response surface method has been used for developing the mathematical model, which can be used to predict the tensile strength and the microhardness of the cast composites at 95 % confidence level. The result indicates that the stirrer blade angle α has the greatest influence on the tensile strength and microhardness followed by N and T .

Keywords Metal matrix composites · Stir casting · Response surface method · Optimization · Tensile strength · Microhardness

1 Introduction

For the past decades, usage of aluminium matrix composites (AMCs) has enormously increased due to its light weight, high specific strength and enriched in mechanical

and thermo physical properties. These are preferred over conventional aluminum alloys in numerous applications owing to their enhanced performance. Exclusively, AMCs play a vital role in modern material science, particularly in all types of transportation, military and structural applications [1]. Researchers developed various techniques to enhance the material behavior of AMCs for the application of defense and aeronautical purposes. Focusing on the distribution of reinforcing particles, good wettability, low porosity, the absence of chemical reactions at the interface and moderate volume fraction makes the AMCs improve their material properties. A variety of production techniques have been developed to reinforce several potential ceramic particles such as fly ash [2], SiO₂ [3], TiO₂ [4], AlN [5], Si₃N₄ [6], TiC [7], B₄C [8], TiB₂ [9] and ZrB₂ [10] with aluminium alloys in order to fabricate AMCs. Among all ceramics, TiC is particularly attractive due to its high hardness, stiffness and wear resistance [11–14]. TiC also improves the properties of aluminium matrix such as ductility, toughness, electrical and thermal conductivity [15–21]. Sharma concluded from his research on the production of Al/TiC AMC by the insitu reaction of K₂TiF₆ salt and particulate graphite that TiC is an effective grain refiner for AMCs [22]. Most of the production techniques are expensive; therefore attempts have been being made to fabricate AMCs at lower cost to enhance the properties of AMCs for similar engineering applications. Liquid, semi-solid and solid state casting routes are used to fabricate the AMCs. Among various techniques, liquid stir casting method is the most potential one for engineering applications in terms of production capacity and cost efficiency. Stir casting techniques are economical, easier to apply and more convenient for mass production compared to other manufacturing techniques [23]. Usually in stir casting, the molten matrix in the furnace is stirred continuously until

✉ S. Joseph Sekhar
josephsekhar@hotmail.com

¹ Department of Mechanical Engineering, St. Xavier's Catholic College of Engineering, Nagercoil, Tamilnadu 629003, India

the vortex is developed. The particle is poured tangentially at a predetermined rate into the periphery of the vortex and the reinforcing particles are entrapped into the matrix due to the centrifugal force developed by the stirrer blade. Mechanical stirrer is introduced to stir the aluminium melt vigorously. Then, the molten metal is poured into the preheated die. The molten metal in the die is allowed to solidify and is further subjected to heat treatment or other secondary processes for enhancing its properties. The stir casting technique is simple and it produces near net shape components and products having many features and irregular contours which can be fabricated using stir casting. Proper selection of process parameters is essential to gain sound AMCs due to micro porosity, poor particle distribution, interfacial reaction and decomposition of ceramic particle [24, 25]. Literatures regarding the production of AMCs are available vastly but, the effect of process parameters has been reported in limited numbers [26–35]. Nai and Gupta reported the increase in the homogeneity of particle distribution within the stirring speed in AA1050/SiCAMCs [26]. Prabu et al. [27] reported the poor particle distribution and clustering at lower stirring speed with lower stirring time in A384/SiC AMCs. Hasim prepared A359/SiC composite with different stirring condition and found that the stirring speed improves the wetting action between the matrix and SiC [28]. Sasaki [29] analyzed the visualized model of glycerin which resembles the property of AZ91D magnesium alloy and concluded that the distance between the blade and liquid surface, the rotational speed of blade and stirring time affect entrapping of gas. Ashok Kumar and Murugan [30] encountered difficulty in the homogeneous distribution of the reinforcing particles into the matrix in stir casting and concluded that the proper selection of blade parameter produces the uniform distribution of reinforcing particles into the matrix. Sozhamannan [31] studied the influence of

process parameters on the metal matrix composites in view of its micro structure study, hardness distribution and density distribution. Zhang et al. [32] investigated the influence of stirring speed, stirring time and casting temperature on the microstructure of Al-6.8 Mg/SiCAMCs and accomplished better distribution of particles. Li-na et al. [33] observed an increase in the homogeneity of reinforcement and tensile properties with a decrease in the stirring temperature and an increase in the stirring time in AA6061/(ABOw + SiCp) hybrid AMCs. Akbari et al. [34] observed an increased porosity content with an increase in stirring time in A356/Al₂O₃ AMCs. Khosravi et al. [35] reported an increase in the porosity content with an increase in stirring speed and casting temperature in A356/SiCAMCs. The process parameters were chosen randomly and their effects were studied with reference to published literatures. Hence, the objective of the present work is to develop an empirical relationship incorporating the stir casting variables to predict the tensile strength and microhardness. Besides, the effects of stir casting variables are deduced from the developed empirical relationship and are correlated.

2 Experimental Procedure

The parameters which influence the stir casting process are presented in Fig. 1. Among all the parameters, the predominant factors having a strong influence on the properties of AMCs are α , N and T . Those factors are chosen in the present study based on the literature survey [26–35].

In spite of the literature survey, experiments were conducted to set the limit, and the micrograph results are given in the Table 1. According to the experimental results, the limits of each factor were decided. The upper and lower limits of a factor were coded as +2 and –2 respectively for

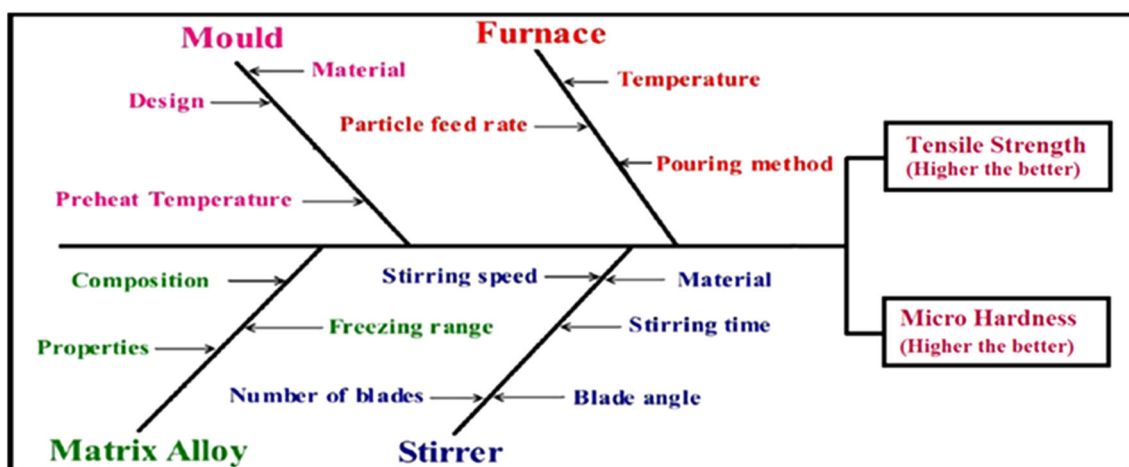
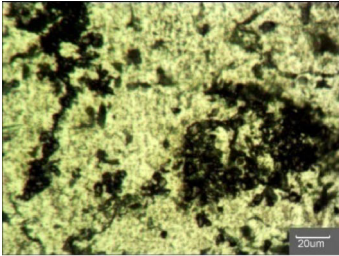
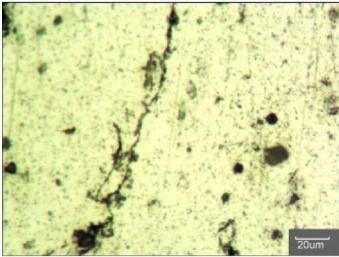
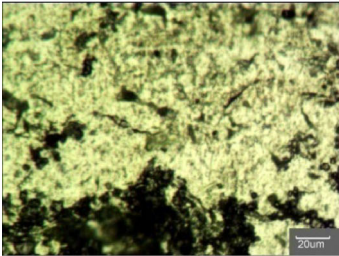
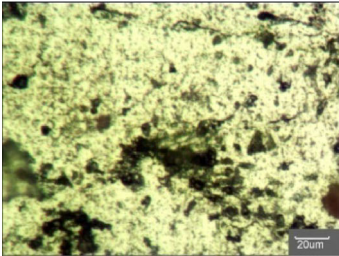


Fig. 1 Stir casting process parameters

Table 1 Microstructure observation for fixing the working range of parameters

Parameter	Range	Microstructure	Type of defect
Stirring Speed	>100		Agglomeration
Stirring Speed	<500		Scattering of particle
Stirring Time	<30		Agglomeration
Blade Angle	<60		Agglomeration

the convenience of recording and processing experimental data. The intermediate values were calculated from the following relationship [44]

$$X_i = 2[2X - (X_{max} + X_{min})]/(X_{max} - X_{min}) \quad (1)$$

where X_i is the required coded value of a variable X ; X is any value of the variable between X_{min} and X_{max} ; X_{min} is the lowest level of the variable; X_{max} is the highest level of the variable. The chosen levels and selected process parameters with their units and notations are presented in Table 2 with all other casting parameters which were maintained constant as in Table 3.

A three factor, five level central composite rotatable factorial design consisting of 20 sets of coded conditions with six center points is presented in Table 4 and was selected to carry out the experiments. A complete description of the design matrix is available in the literatures [36, 37]. Aluminum alloy AA6061 was used as the matrix alloy and the measured quantity of AA6061 rods were placed into the furnace crucible. The chemical composition of AA6061 is shown in Table 5. An electric resistance furnace was used to melt the alloy of AA6061 rod. The mechanical stirrer was introduced and immersed into the furnace crucible at 2/3 of

Table 2 Stir casting parameters and their levels

*	Parameter	Notation	Levels				
			−1.682	−1	0	1	1.682
1	Blade angle (°)	α	0	15	30	45	60
2	Stirrer speed (rpm)	N	100	200	300	400	500
3	Stirring time (min)	T	5	10	15	20	25

Table 3 Constant stir casting parameters and their values

*	Parameter	Value/material
1	TiC feed rate (g/min)	30
2	TiC content (wt%)	15
3	TiC preheat temperature (°C)	600
4	TiC preheat duration (min)	60
5	Wettability agent	Magnesium
6	Amount of wettability agent (wt%)	2
7	Number of stirrer blades	3
8	Stirrer material	Graphite
9	Preheat temperature of die (°C)	250
10	Die material	Tool steel
11	Furnace atmosphere	Argon
12	Furnace temperature	650 °C

the total height of aluminum melt. The mechanical stirrer with different blade angles which was made up of graphite material is shown in Fig. 2. TiC particles were gradually fed tangentially into the vortex and stirred continuously. While reinforcing the TiC particles into the vortex, the temperature of the furnace was increased by about 10 °C to maintain liquidity. The morphology of the TiC particles is shown in Fig. 3. Titanium carbide powder of average size 2 μm was taken for this study and it was subjected to heat treatment for about 1 h at 600 °C in order to enhance the wettability of AA6061 and TiC. The particles of sizes <10 μm would suspend in the aluminum melt for a long time and would be least influenced by gravity [24]. Moreover the magnesium was incorporated into the aluminium melt to improve the wetting action. Inert gas argon was provided into the furnace while processing to prevent the formation of aluminium oxide. The molten AMC was then poured into the preheated die of about 250 °C through gravity die casting method and allowed to solidify at ambient condition. Castings were carried out randomly as per the design matrix.

Tensile specimens from each trial run of the casting were prepared as per the ASTM E8M standard having a gauge length, width and thickness of 40, 7 and 6 mm respectively and the ultimate tensile strength was recorded using computerized universal testing machine (HITECH

TUE-C-1000). The Microhardness tester (MITUTOYO-MVK-H1) was used to record the microhardness of the prepared samples for about 15 s with 5 N applied load. The mean value of each specimen was taken into account for developing an empirical relationship.

The response function representing the tensile strength and microhardness of the AA6061/TiC composites can be expressed as:

$$R = f(\alpha, N, T) \quad (2)$$

The second order polynomial regression equation used to represent the response surface 'Y' for κ factor is given by

$$Y = b_0 + \sum_{i=1}^k b_i x_i + \sum_{i=1}^k b_{ii} x_i^2 + \sum_{i=1}^k b_{ij} x_i x_j \quad (3)$$

The selected polynomial for three factors can be expressed for all the responses as:

$$R = b_0 + b_1 \alpha + b_2 N + b_3 T + b_{11} \alpha^2 + b_{22} N^2 + b_{33} T^2 + b_{12} \alpha N + b_{13} \alpha T + b_{23} NT \quad (4)$$

where b_0 is the average of responses and b_1, b_2, \dots, b_{23} are the response coefficients that depend on the main and interaction effects of the parameter. Using SYSTAT 12 software, the coefficients were calculated and the empirical relationships were developed after determining the coefficients which were subsequently tested for their significance at 95 % confidence level. The developed empirical relationship to predict the tensile and microhardness of the casted composites are given below in Eqs. 5 and 6.

$$\begin{aligned} \text{Tensile strength} = & 229.25 + 7.472\alpha + 1.687N + 2.280T \\ & - 30.753\alpha^2 - 18.028N^2 \\ & - 16.968T^2 \text{ MPa} \end{aligned} \quad (5)$$

$$\begin{aligned} \text{Microhardness} = & 108.972 + 8.943\alpha + 2.326N + 1.541T \\ & - 20.033\alpha^2 - 8.369N^2 - 5.895T^2 \text{ HV} \end{aligned} \quad (6)$$

The statistical relations for the developed empirical relationship are presented in the Table 3. If the R square

Table 4 Design matrix and experimental result

Trial run	Design matrix			Tensile strength (MPa)	Micro hardness (HV)
	α	N	T		
T1	-1	-1	-1	131	45
T2	-1	-1	1	149	56
T3	-1	1	-1	146	54
T4	-1	1	1	188	87
T5	1	-1	-1	155	67
T6	1	-1	1	164	73
T7	1	1	-1	162	71
T8	1	1	1	193	94
T9	-1.682	0	0	181	85
T10	1.682	0	0	203	99
T11	0	-1.682	0	183	90
T12	0	1.682	0	201	98
T13	0	0	-1.682	194	95
T14	0	0	1.682	209	103
T15	0	0	0	220	108
T16	0	0	0	219	107
T17	0	0	0	220	108
T18	0	0	0	216	106
T19	0	0	0	215	105
T20	0	0	0	217	106

value was <1 , then the developed empirical relation was adequate and the predicted empirical relationship values would precisely match with the experimental result. Higher value of R square and lower value of standard error indicated the adequacy of the empirical relationship. The analysis of variance (ANOVA) technique was used to analyse all the responses and is presented in Table 4. The calculated F ratio was higher than the tabulated F ratio values at 95 % confidence level which showed the developed empirical relationships which were adequate. Besides, the scatter diagrams were drawn corresponding to the experimental values and predicted values in the Fig. 4. The experimental values were scattered both sides and close to 45° inclined line of predicted values showing the adequacy of the empirical relationships.

Four tests were conducted at different values of α , N and T other than those used in the design matrix and their responses were estimated and shown in Table 6 which confirmed the validity of the developed empirical relationships. The percentage of error was calculated as

$[(\text{experimental value} - \text{predicted value})/\text{predicted value}] \times 100$ and the percentage of error did not exceed ± 5 % which confirmed the accuracy of the developed empirical relationships [38, 39]. The specimens from selected castings were prepared and polished using standard metallographic technique, further etched with Keller's reagent and the microstructure were studied using scanning electron microscope (SEM, JEOL-JSM-6390).

3 Results and Discussion

The effects of process parameters such as α , N and T on the UTS and microhardness of AA6061/TiC are evaluated using the developed empirical relationships and the predicted trends are shown in Figs. 5, 6 and 7. The effects of the process parameters and the possible causes are elaborated in the following sections.

3.1 Effect of Blade Angle

The TiC particles reinforced into the aluminium alloy AA6061 have a satisfactory effect in improving the tensile strength as well as hardness of the composite. Figure 5 reveals the effect of blade angle on tensile strength and microhardness of AMC at a constant stirring speed of 300 rpm and stirring time of 15 min. At lower blade angle, the tensile strength and microhardness are lower and increases up to the blade angle 30° and then suddenly, the curve descends towards the higher value. The particle distribution that is clustered in a particular place and absent in some other space shows remarkable change in microhardness at a different location of the specimen, and during tensile loading crack develops in the region where the particles are absent. The swirl generated by the stirrer rotation decides the distribution of particles within the melt. In order to achieve homogeneity of the particle distribution, the axial and radial variation of the currents should be shorter in range. Besides, an optimum inclination of the stirrer blade is required to disperse the particles uniformly into the melt [40–43]. Lower blade angles cause the TiC particles to sediment near the wall and bottom of the crucible. Higher blade angles cause the particles concentrate at the apex of the vortex resulting in radial variation. The stirrer blade angle refers to the inclination of the blade with respect to the horizontal plane which is perpendicular to the axis of the crucible. Balance in radial as

Table 5 Chemical composition of AA 6061

Element	Si	Fe	Cu	Mn	Mg	Zn	Ti	Cr	Al
wt%	0.4–0.8	0.7	0.15–0.4	0.15	0.8–1.2	0.25	0.15	0.04–0.35	Balance

Fig. 2 Stirrer blade angle **a** 0°, **b** 15°, **c** 30°, **d** 45°, **e** 60°

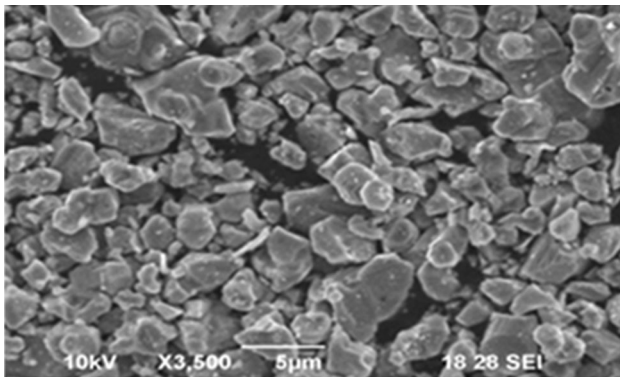
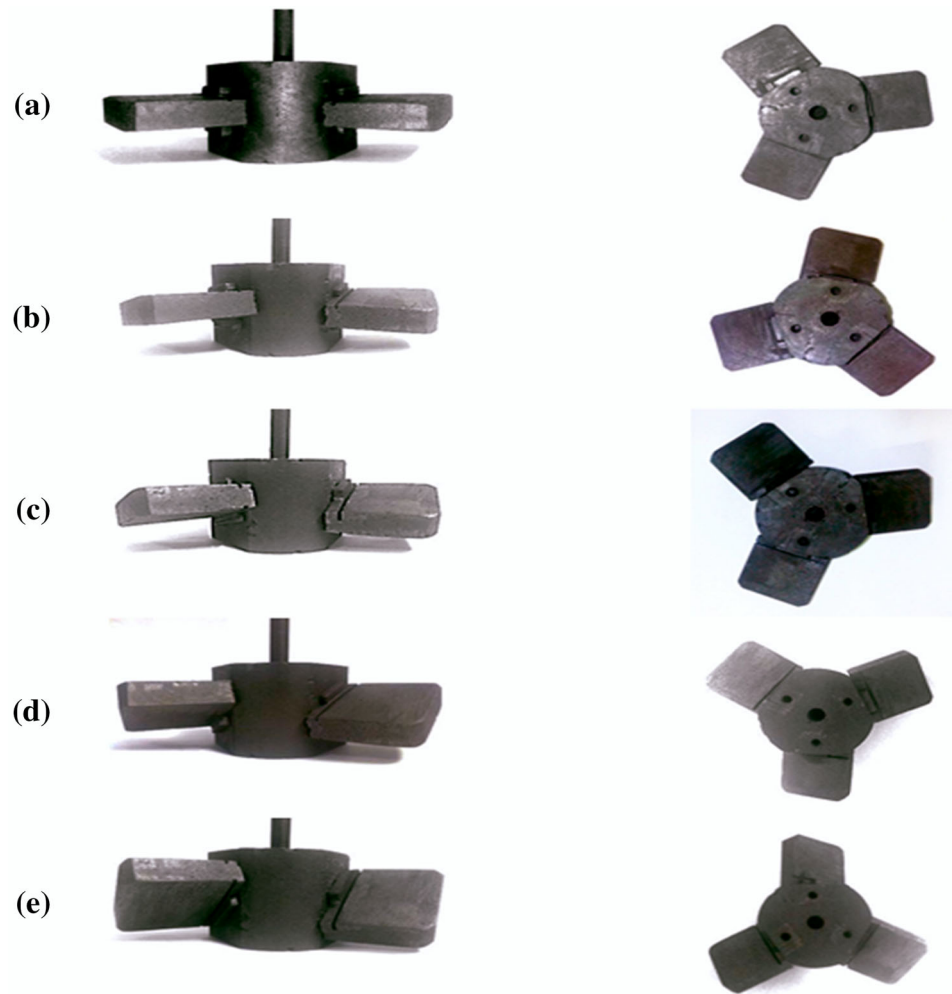


Fig. 3 FESEM image of TiC powder

well as axial flow results in uniform distribution of the particles.

The blade angle provokes the angular flow which generates a variation in the axial and radial currents. Figure 8 shows the micrograph of AA6061/TiCAMC at various blade angles. The difference in the micrograph shows the

influence of the blade angle. Formation of clusters of TiC particles and free regions are observed at blade angle 0° which reveals that the development of the vortex is not enough for sufficient particle incorporation. The current induced by the blade angle 0° is relatively low and this centrifugal current leads to poor distribution, which results in cluster formation. The micrograph reveals the non-homogeneous distribution of the TiC particles made by stirrer blade angle 0°. Figure 8b shows the homogeneous distribution of the TiC particles in the aluminium matrix at 30° stirrer blade angle, where no clusters formation is seen. The result indicates that placing the stirrer blade in different orientation influences the TiC particle distribution. The angular velocity of the aluminium melt increases by the stirrer blade angle which leads to an increase in the centrifugal current within the melt. These currents forces the particles to get scattered from the clusters of TiC in the aluminum melt which results in uniform distribution. The micrographs (Fig. 8c, d) show the top and bottom of the casting at stirrer blade angle 60°. The distribution of the

Fig. 4 Scatter diagram of developed model

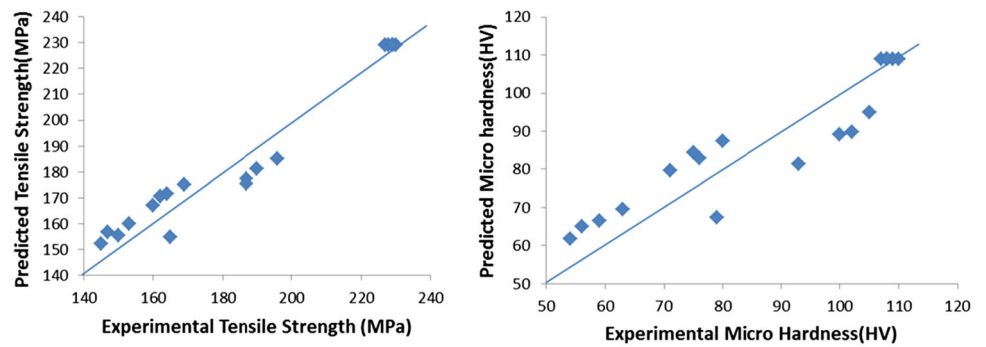


Table 6 Result of conformity experiment

Trial run	Casting process parameters			Tensile strength (MPa)			Micro hardness (HV)		
	α	N	T	Actual	Predicted	Error (%)	Actual	Predicted	Error (%)
1	-0.9	-0.7	-0.9	153	154	-0.65	62	61	1.64
2	-0.4	-0.3	-0.4	206	205	0.49	94	93	1.08
3	0.2	0.1	0.2	230	228	0.88	111	110	0.91
4	0.8	0.6	0.7	217	214	1.40	103	104	-0.96
Average						0.53			0.67

Fig. 5 Effect of blade angle on UTS and microhardness of AA6061/TiC at $N = 300$ rpm and $T = 15$ min

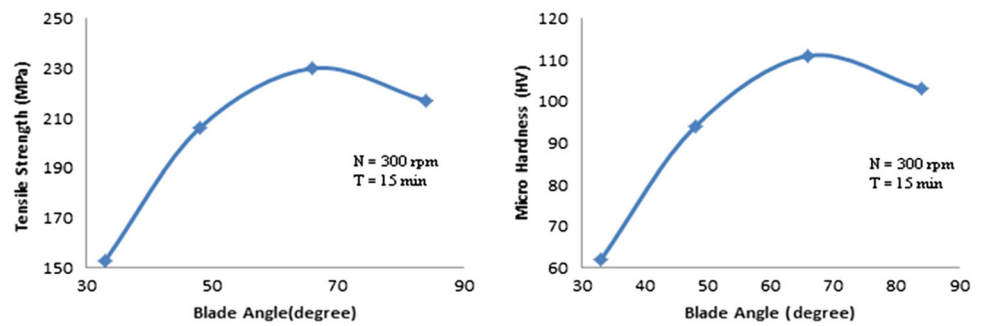
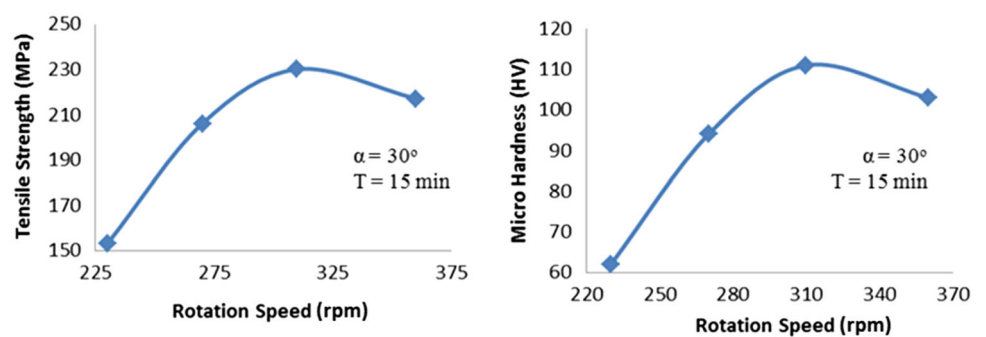


Fig. 6 Effect of stirring speed on UTS and microhardness of AA6061/TiC at $\alpha = 30^\circ$ and $T = 15$ min



particles is not alike in both micrographs and a few particles are observed (Fig. 8c) at the top of the casting, and homogeneous distribution of TiC particles are observed at the bottom of the casting (Fig. 8d) owing to different

magnitude in centrifugal currents. This reveals that the angular velocity is high at 60° blade angle and due to that the TiC particles are pushed towards the bottom of the crucible and the interparticle distance is closer to each

Fig. 7 Effect of stirring time on UTS and microhardness of AA6061/TiC at $\alpha = 30^\circ$ and $N = 300$ rpm

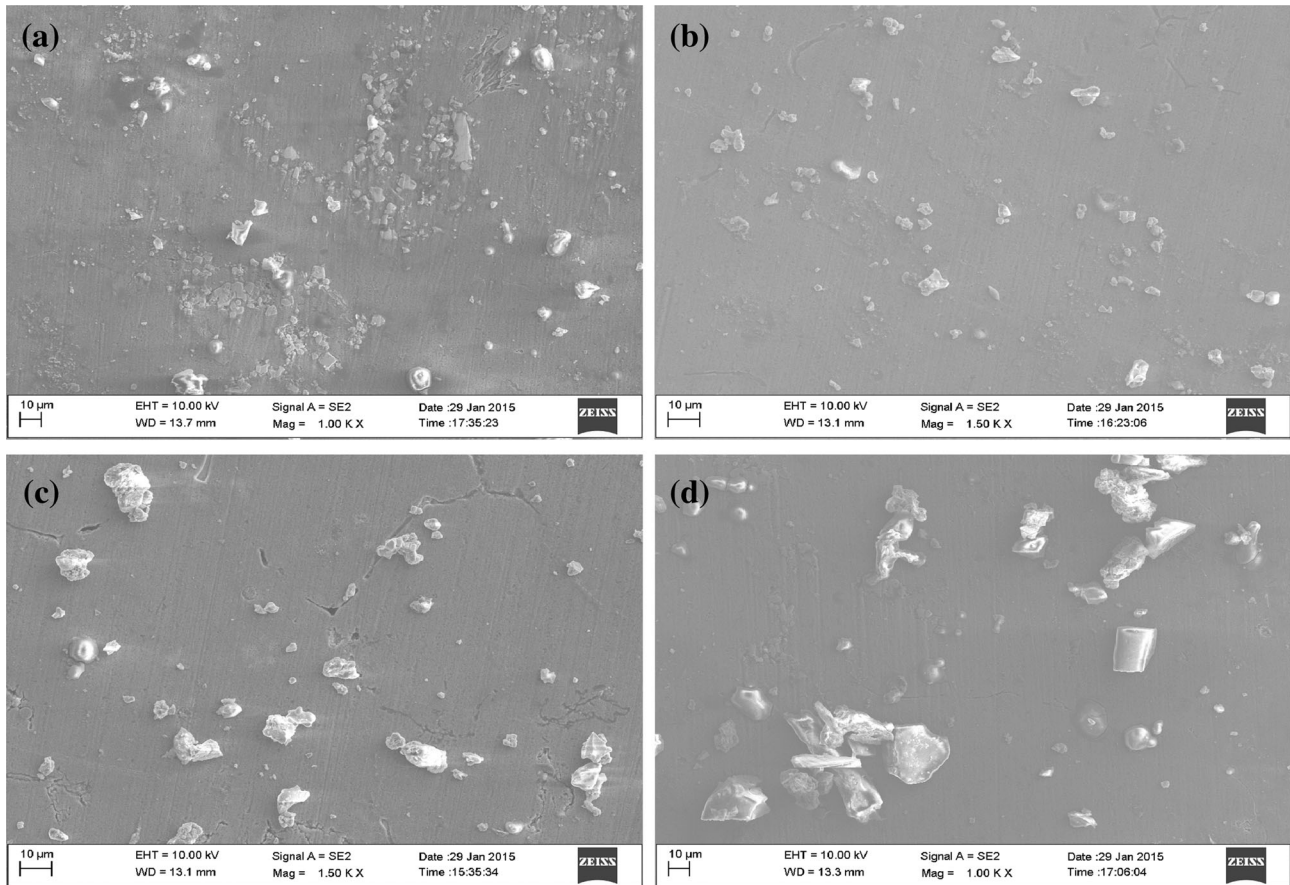
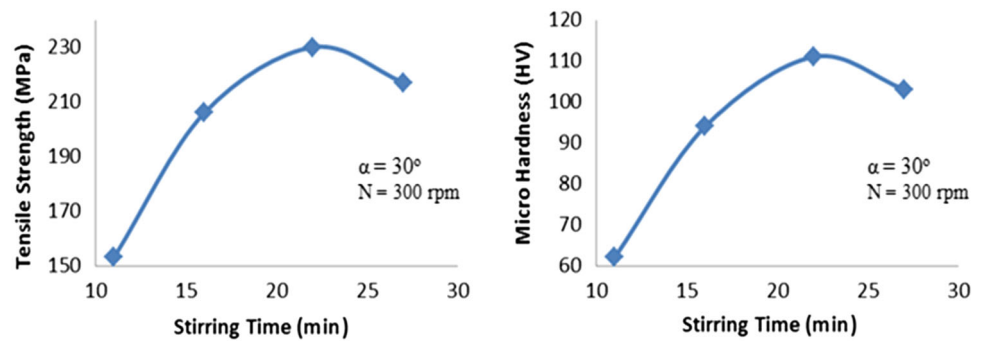


Fig. 8 FESEM micrograph of AA6061/TiC AMC at blade angle of **a** 0° , **b** 30° , **c** 60° (top portion of casting) and **d** 60° (bottom portion of casting)

other when compared to the micrograph, (Fig. 8b), of blade angle 30° . Naher et al. [40] also reported similar observations. The micro porosity is also observed from the micrographs (Fig. 8c) which shows the intense swirl dragging the TiC particles towards the bottom of the crucible together with more air entrapment into the aluminium melt, and leads to micro voids during solidification. The optimum homogeneous distribution of the TiC particles is observed at the blade angle 30° .

3.2 Effect of Stirring Speed

Figure 6 shows the predicted result of stirrer speed on the properties of AA6061 for a given stirring time of 15 min and blade angle 30° . The properties of AA6061 increases as stirrer speed increases and attain a maximum at 300 rpm. When the stirrer speed increases further, the vortex height also increases due to the centrifugal current. TiC particle is fed into the vortex

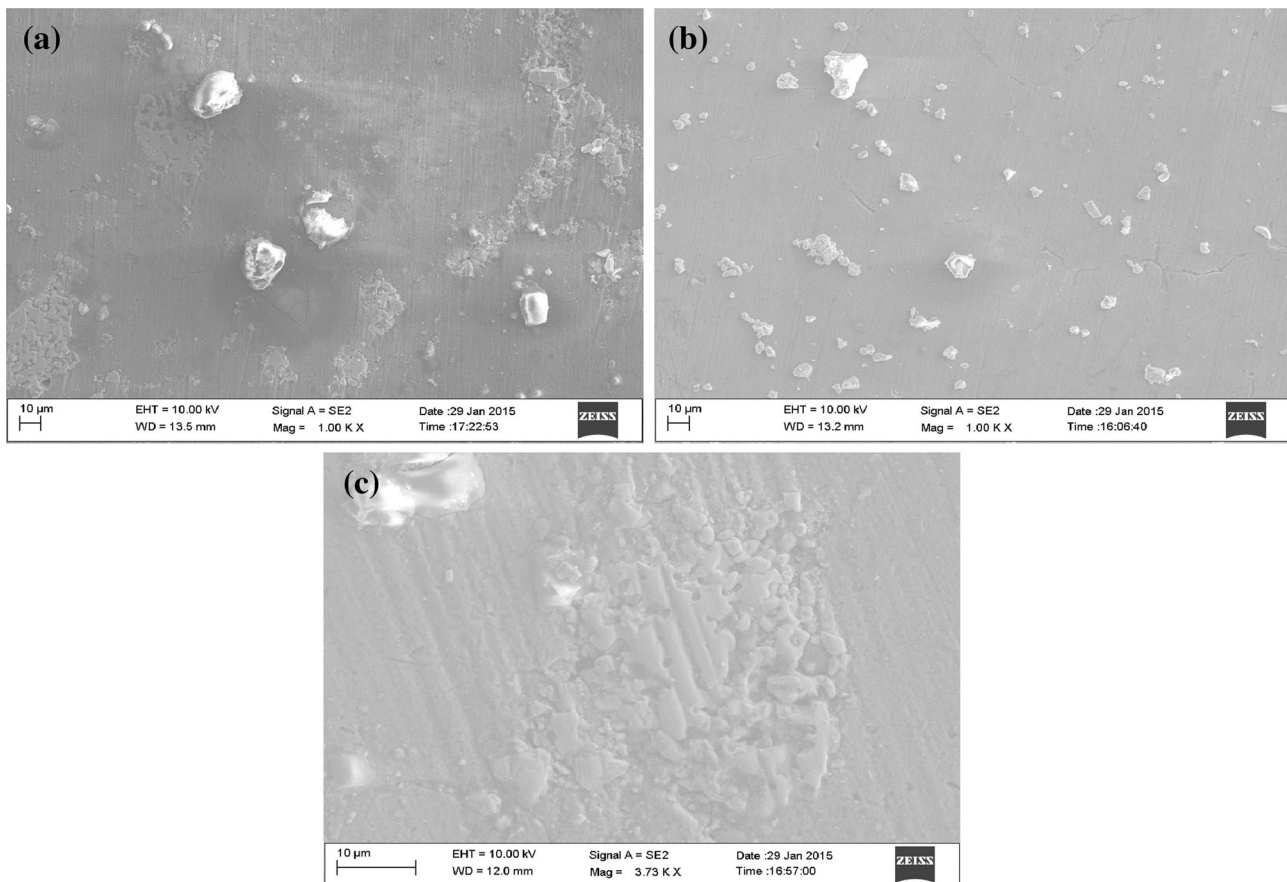


Fig. 9 FESEM micrograph of AA6061/TiC AMC at stirring speed of **a** 100 rpm, **b** 300 rpm and **c** 500 rpm

during its formation, and thus the unbalancing of angular flow in aluminum melt causes the reinforcing particle to scatter vigorously towards the inner wall of the crucible. After pouring the melt into the die, solidification takes place and limited particles are entrapped in the aluminum alloy 6061 which retards enhancement in properties of AMC.

When the stirring speed is at 300 rpm, the size of the vortex formation is strong enough to mix the particles and keep the particles suspended for longer duration.

The magnitude of the circulating current and the size of the vortex depend on stirring speed. The micrographs of AA6061/TiC AMCs at various speeds are represented in Fig. 9. At a lower speed of 100 rpm, the distribution of the particle is limited and there is a lack of TiC particles in some region, besides clusters of TiC particles are seen in other region which denotes that the produced vortex and lower circulating current are insufficient to result in homogeneous distribution. Collection of clusters, particle free regions and poor distributed regions are observed in the micrograph. On the other hand, formation of deep vortex and high circulating current at higher stirring speed results

in turbulence which introduces entrapped air into the melt and produces porosity. This is evident from the micrograph (Fig. 9a). The micrograph at 300 rpm, (Fig. 9b) shows the homogeneous distribution of TiC particles. The vortex formation and centrifugal current produced at 300 rpm disintegrate the TiC clusters into the aluminium melt which results in homogenous distribution of particles. When the stirring speed is increased to 500 rpm, it tends to increase the interparticle distance and also the region of porosity which is observed from the micrograph (Fig. 9c). The porosities observed in stir cast AMCs are of four types; (a) porosity associated with individual particle; (b) porosity associated with particle clusters; (c) micro porosity in the aluminum matrix and (d) gas porosity [26]. A deep vortex and high circulating current, not only causes the homogeneous distribution but also an increase in interparticle distance. This leads the air present in the atmosphere to get entrapped into the aluminium melt due to high pressure difference. During solidification, the entrapped gas does not get relieved completely from the AMC casting which causes pore formation. The porosity is not observed at the stirring speed of 100 and 300 rpm.

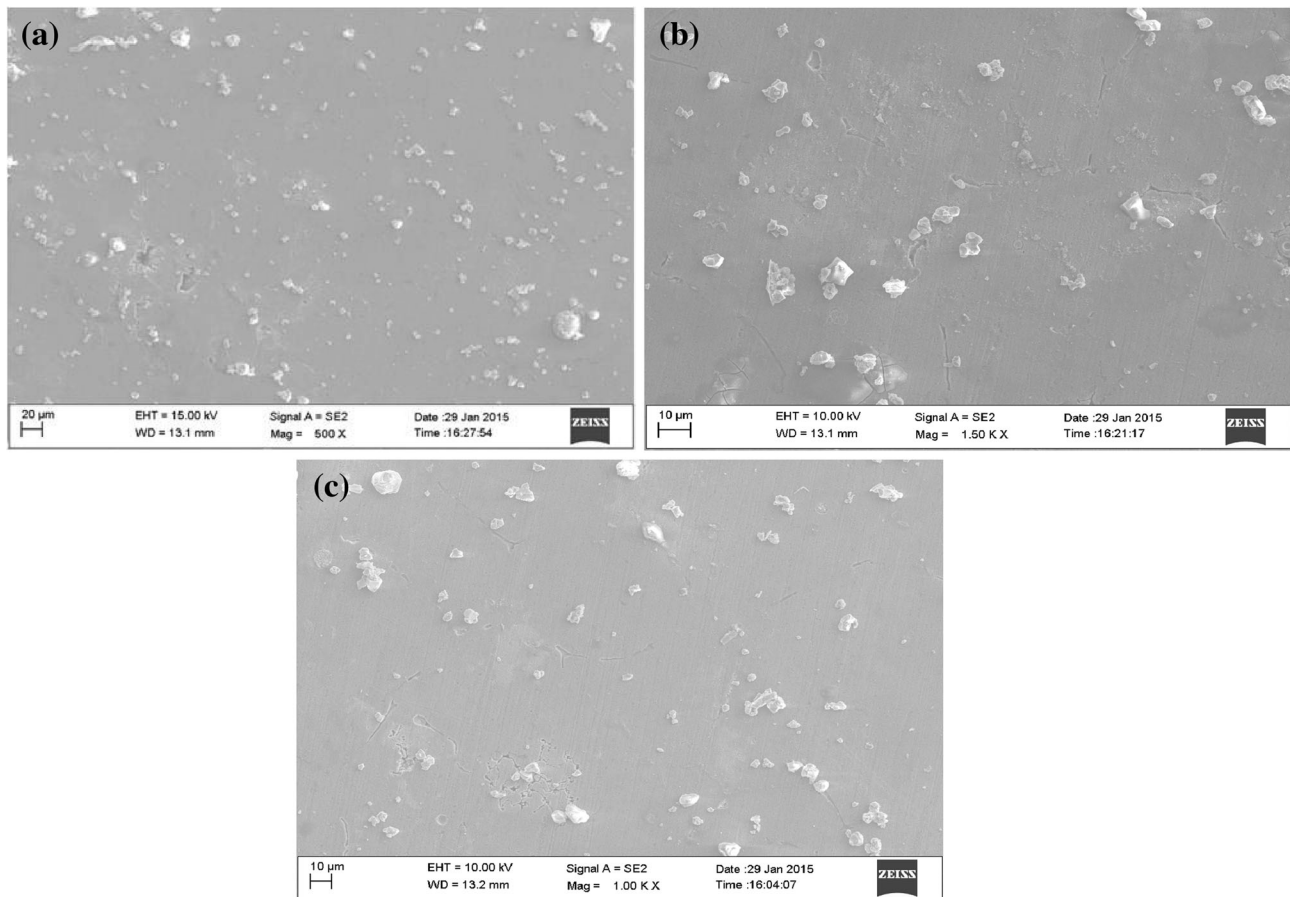


Fig. 10 FESEM micrograph of AA6061/TiC AMC at stirring time of **a** 5 min, **b** 15 min and **c** 25 min

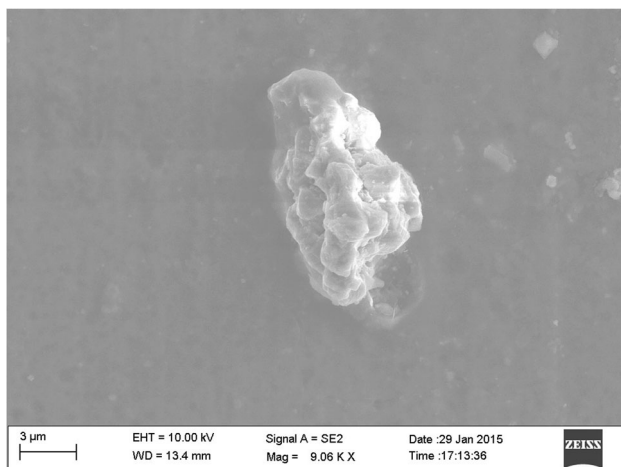


Fig. 11 FESEM micrograph of AA6061/TiC AMC

3.3 Effect of Stirring Time

The predicted effect of stirring time on the properties of AA6061/TiC is depicted in Fig. 7 for a stirring speed of 300 rpm and blade angle 30°. The properties of AMC

enhance as stirring time increases and reaches maximum at 15 min. The properties are reduced by further increase in the stirring time. The formation of vortex due to the stirring action forces the particle to get entrapped into the aluminium melt and the fed particles will not disperse into all regions of the aluminium melt at once. Hence continuous stirring is needed to disperse the particles uniformly. The dispersion is a function of time [27]. Homogeneous dispersion through the aluminium melt can be achieved by producing constant centrifugal currents over a definite period of time. Besides, the amount of entrapped air depends upon the stirring time with respect to the vortex formation which leads to porosity. Excess stirring time tends to entrap excessive air into the aluminium melt. The micrographs of AA6061/TiC AMC casting at various stirring time is depicted in Fig. 10. During stirring time of 5 min the micrograph, (Fig. 10a) shows huge amount of clusters at one region and particle free zone in other region which concludes that the stirring time is insufficient to disperse the TiC particles uniformly into the aluminium melt. Integration of TiC particles in the aluminium melts results in cluster formation. The micrograph (Fig. 10b) at stirring time of 15 min represents the homogeneous

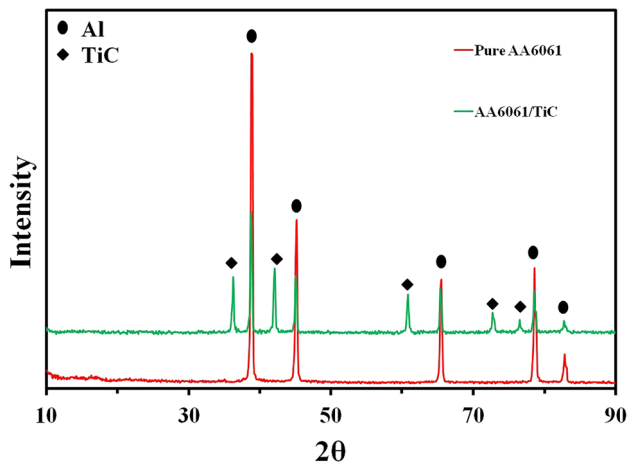


Fig. 12 XRD of pure AA6061 and AA6061/TiC

distribution of TiC particles in the aluminium matrix and no cluster formation is observed. The stirring time of 15 min causes the particles fall in uniform distribution due to the centrifugal currents within the molten aluminium which disintegrate the clustering of TiC particles and the particles are driven away towards particle free regions. The inter-particle distance also increases at the stirring time of 15 min. The micrograph (Fig. 10c) at stirring time of 25 min shows homogeneous distribution of TiC particles along with porosity. Various types of porosities and their causes have been discussed previously. Longer stirring time produces more agitation in the molten composite which increases the tendency to form more porosity [34]. Figure 11 shows the particle shape, size and the clear interface between the matrix and TiC particle. No interfacial reactions are observed. When the composite is subjected to tensile load, the applied load in the matrix is transferred to the TiC particle and this acts as a load barrier which promotes the property enhancement in the AMC. The XRD graph is presented in Fig. 12, which shows the peaks of aluminium and TiC. No peaks of interfacial reaction compounds such as Al_3Ti , Al_3C_4 , Al_2O_3 are observed and also the XRD confirms the integrity of TiC particles during casting. The micro hardness and UTS are high when the microstructure shows homogenous distribution of TiC particles. The optimum uniform distribution of TiC particles with least porosity is observed for stirring time of 15 min, while a longer stirring time or a lower stirring time scatters the desired microstructure.

4 Conclusions

In the present work, specimens of AA6061/15 %wt. TiC AMC have been fabricated successfully using stir casting technique. Empirical relationships incorporating the stir

casting parameters have been developed to predict the properties such as the ultimate tensile strength and microhardness of AMC. It is observed that stirrer blade angle, stirring speed and stirring time are the major stir casting parameters which influences the properties of AMC. Based on the various results obtained, the following conclusions are drawn:

1. The levels of process parameters result in low UTS and also microhardness, besides formation of clusters, porosity and agglomeration of TiC particles are present at grain boundaries.
2. At stirring blade angle of 30° , stirring speed of 300 rpm and stirring time of 15 min produces homogenous distribution of TiC particles with minimum porosity.
3. Higher level of process parameters (>0) yields better distribution of TiC particles with high porosity which is preferred to fabricate uniform distribution of TiC particles.
4. The optimized parameters reveal that the intermediate process parameters produces better distribution of TiC particles with minimal porosity.

References

1. Gopalakrishnana S, and Murugan N, *Compos Part B Eng* **43** (2012) 302.
2. Robinson Smart D S, David Raja Selvam J, and Dinaharan I, *Mater Des* **49** (2013) 28.
3. Hemanth J, *Compos Part B Eng* **42** (2011) 1826.
4. Sivasankaran S, Sivaprasad K, Narayanasamy R, and Iyer V K, *Powder Technol* **201** (2010) 70.
5. Liu Z Y, Kent D, and Schaffer GB, *Mater Sci Eng A* **513–514** (2009) 352.
6. Moghaddas M A, and Bozorg S F K, *Mater Sci Eng A* **559** (2013) 187.
7. Wu Q, Yang C, Xue F, and Sun Y, *Mater Des* **32** (2011) 4999.
8. Mindivan H, *Mater Lett* **64** (2010) 405.
9. Niranjana K, and Lakshminarayanan P R, *Mater Des* **47** (2013) 167.
10. Dinaharan I, and Murugan N, *Trans Nonferrous Met Soc China* **22** (2012) 810.
11. Kennedy A R, and Wyatt S M, *Compos A* **32** (2001) 555.
12. Padney A B, Mishra R S, and Mahajan Y R, *Mater Sci Eng A*, **A206** (1996) 270.
13. Jiang W H, Song G H, Han X L, He C L, and Ru H C, *Mater Lett* **32** (1997) 63.
14. Li P, Kandalova E G, Nikitin V I, Makarenko A G, Luts A R, and Yanfei Z, *Scr Mater* **49** (2003) 699.
15. Sahoo P, Koczak M J, *Mater Sci Eng A* 131 (1991) 69.
16. Nakata H, Choh T, and Kanetake N, *J Mater Sci* **30** (1995) 1719.
17. Mitra R, Chiou W A, Fine M E, and Weertman J R, *J Mater Res* **8** (1993) 2380.
18. Mitra R, Weertman J R, and Fine M E, *J Mater Res* **8** (1993) 2370.
19. Shipway P H, Kennedy A R, and Wilkes A J, *Wear* **216** (1998) 160.
20. Kennedy A R, Karantzalis A E, and Wyatt S, *J Mater Sci* **34** (1999) 933.

21. Karantzalis E, Wyatt S, and Kennedy A R, *Mater Sci Eng A* **237** (1997) 200.
22. Sharma A, *Int J Cast Met Res* **21** (2008) 226.
23. Taha M A, *Mater Des* **22** (2001) 431.
24. Hashim J, Looney L, and Hashmi M S J, *J Mater Proc Technol* **123** (2002) 251.
25. Hashim J, Looney L, and Hashmi M S J, *J Mater Proc Technol* **123** (2002) 258.
26. Nai S M L, and Gupta M, *Compos Struct* **57** (2002) 227.
27. Prabu S B, Karunamoorthy L, Kathiresan S, and Mohan B, *J Mater Proc Technol* **171** (2006) 268.
28. Hashim J, Looney L, and Hashmi M S J, *J Mater Proc Technol* **119** (2001) 329.
29. Sasaki G, Yosida M, Fuyyama N, and Fujii T, *J Mater Proc Technol* **130–131** (2002) 151.
30. Ashok Kumar B, and Murugan N, *Mater Des* **40** (2012) 52.
31. Sozhamannan G G, Balasivanandha Prabhu S, and Venkatagalapathy V S K, *J Surf Eng Mater Adv Technol* **2** (2012) 11
32. Zhang H, Geng L, Guan L, and Huang L, *Mater Sci Eng A* **528** (2010) 513.
33. Li-na G, Lin G, Hong-wei Z, and Lu-jun H, *Trans Nonferrous Met Soc China* **21** (2011) s274.
34. Akbari M K, Mirzaee O, and Baharvandi H R, *Mater Des* **46** (2013) 199.
35. Khosravi H, Bakhshi H, and Salahinejad E, *Trans Nonferrous Met Soc China* **24** (2014) 2482.
36. Box G E P, Hunter W H, and Hunter J S, *Statistics for Experiments*, Wiley, New York (1978).
37. Montgomery D G, *Design and Analysis of Experiments*, Hoboken, Wiley (2001).
38. Barmouz M, and Givi M K B, *Compos Part A* **42** (2011) 1445.
39. Barmouz M, Givi M K B, and Jafari J, *Adv Mater Res* **154–155** (2011) 1761.
40. Naher S, Brabazon D, and Looney L, *J Mater Proc Technol* **143–144** (2003) 567.
41. Ravi K R, Sreekumar V M, Pillai R M, Mahato C, Amaranathan K R, Arul Kumar R, Pai BC, *Mater Des* **28** (2007) 871.
42. Rohatgi P K, Sobczak J, Asthana R, and Kim J K, *Mater Sci Eng A* **252** (1998) 98.
43. Bui R T, Ouellet R, and Kocafe D A, *Metall Mater Trans B* **25** (1994) 607.
44. Miller I, Freund J E, and Johnson, *Probability and Statistics for Engineers*, Prentice of Hall of India, New Delhi (1999).